POLARIMETRIC SAR TOMOGRAPHY WITH TERRASAR-X BY MEANS OF DISTRIBUTED COMPRESSED SENSING

E. Aguilera, M. Nannini, A. Antonello, L. Marotti, P. Prats, and A. Reigber

Microwaves and Radar Institute, German Aerospace Center (DLR) P.O. Box 1116, 82230 Wessling, Germany

ABSTRACT

In SAR tomography, the vertical reflectivity function for every azimuth-range pixel is usually recovered by processing data collected using a defined repeat-pass acquisition geometry. A common and appealing approach is to generate a synthetic aperture in the elevation direction through imaging from parallel tracks. However, the quality of conventional reconstruction methods is generally dictated by the Nyquist rate, which can be considerably high. In an attempt to reduce this rate, we propose a new tomographic focusing approach that exploits correlations between neighboring azimuth-range pixels and polarimetric channels. As a matter of fact, this can be done under the framework of Distributed Compressed Sensing (DCS), which stems from Compressed Sensing (CS) theory, thus also exploiting sparsity in the tomographic signal. Results demonstrating the potential of the DCS methodology will be validated, for the first time, using dual-polarized data acquired at X-band by the TerraSAR-X spaceborne system.

Keywords: SAR tomography, polarimetry, compressed sensing, distributed compressed sensing.

1. INTRODUCTION

1.1. Compressed sensing

Compressed Sensing (CS) proposes measuring a signal f by collecting m linear measurements of the form $b = Af + y$, where A is a m by n sensing matrix with m typically smaller than n by several orders of magnitude and y is a noise term. The theory asserts that if f is approximately sparse in a specific basis Ψ, it is indeed possible to recover f, under suitable conditions on the matrix A, by L_1 minimization

$$\min_{\widetilde{f}} \left\| \Psi \widetilde{f} \right\|_1 \text{ subject to } \left\| A\widetilde{f} - b \right\|_2 \leq \varepsilon; \qquad (1)$$

where ε is an upper bound on the noise level [3], [1], [5], [4]. In other words, CS thrives on sparse representations to recover a high-resolution signal from a reduced set of samples.

1.2. Distributed compressed sensing

Distributed Compressed Sensing (DCS) theory enables the joint recovery of multi-signal ensembles by exploiting inter-signal correlations. It generalizes the concept of a signal being sparse in some basis to the concept of an ensemble of signals being jointly sparse. In this paper, we demonstrate how to apply a multiple measurement vector model that has been thoroughly studied and can be found in the literature [2], [6]. One of the crowning achievements of this model is that it allows for a further reduction in the number of measurements.

1.3. Compressed sensing for SAR tomography

In [9], CS inversion techniques for SAR tomography have proven to be applicable. The contribution of this paper is to extend this concept and take advantage of the inter-signal correlations between neighboring azimuth-range pixels as well as between polarimetric channels by means of DCS.

2. PROBLEM FORMULATION

Given three 3-D complex reflectivity functions $g_{hh}(x, r, s)$, $g_{vv}(x, r, s)$, and $g_{hv}(x, r, s)$ (one per polarimetric channel) of a specific area; where x, r, and s are the azimuth, range, and elevation coordinates, respectively, and taking a small discretized subset of the space domain, i.e. a window of size Δx, Δr, Δs, so that $1 \leq x \leq \Delta x$, $1 \leq r \leq \Delta r$, and $1 \leq s \leq \Delta s$, is there a way to compress these reflectivity functions? Do they share any information? If so, we can use this knowledge to recover them by means of the DCS machinery. Throughout this paper, the reflectivity functions will be represented as an ensemble of $P = \Delta x \Delta r$ signals along s. That is, $g_{hh}(p, s)$, $g_{vv}(p, s)$, and $g_{hv}(p, s)$ with $1 \leq p \leq P$. Each signal of size Δs will be denoted with the corresponding column vectors g_{hhp}, g_{vvp}, and g_{hvp}. Additionally, the tomographic sensing operation (using parallel tracks) for the signals in the xy channel, will be jointly expressed as

$$B_{xy} = \widehat{\Phi} G_{xy} + Y_{xy}; \qquad (2)$$

where

$$B_{xy} = \begin{bmatrix} b_{xy1} \\ b_{xy2} \\ b_{xy3} \\ \vdots \\ b_{xyP} \end{bmatrix} \tag{3}$$

and

$$\widehat{\Phi} G_{xy} = \begin{bmatrix} \Phi_1 & 0 & 0 & \cdots & 0 \\ 0 & \Phi_2 & 0 & \cdots & 0 \\ 0 & 0 & \Phi_3 & \cdots & 0 \\ \vdots & \vdots & \vdots & \ddots & \vdots \\ 0 & 0 & 0 & \cdots & \Phi_P \end{bmatrix} \begin{bmatrix} g_{xy1} \\ g_{xy2} \\ g_{xy3} \\ \vdots \\ g_{xyP} \end{bmatrix}. \tag{4}$$

The matrices Φ_p, with $1 \leq p \leq P$, are the so-called steering matrices, b_{xyp} is a stack (column vector) of m pixels taken from m corregistered SAR images that are measurements of g_{xyp}, and Y_{xy} is a noise term. Expressions for the different polarimetric channels can be found by replacing xy with hh, vv, or hv, accordingly. Also, $\widetilde{k}$ will represent a vector or matrix of variables to be determined that approximate k. Finally, the support of a vector w is defined as $supp\, w = \{j, w_j \neq 0\}$.

3. COMMON SUPPORT REGULARIZATION

In this method, we suppose that all P signals throughout polarimetric channels share, approximately, the same sparse support in the space domain but have different nonzero coefficients. This makes sense, as we are expecting backscatter from the same structure [7]. From (2), it follows that

$$\begin{bmatrix} B_{hh} \\ B_{vv} \\ B_{hv} \end{bmatrix} = \begin{bmatrix} \widehat{\Phi} & 0 & 0 \\ 0 & \widehat{\Phi} & 0 \\ 0 & 0 & \widehat{\Phi} \end{bmatrix} \begin{bmatrix} G_{hh} \\ G_{vv} \\ G_{hv} \end{bmatrix} + \begin{bmatrix} Y_{hh} \\ Y_{vv} \\ Y_{hv} \end{bmatrix} \tag{5}$$

or $B = \widehat{\Phi}_{all} G + Y$. And so, we can focus in all channels simultaneously by mixed $L_{2,1}$ minimization as follows

$$\min_{\widetilde{H}} \left\| \widetilde{H} \right\|_{2,1} \text{ subject to } \left\| \widehat{\Phi}_{all} \widetilde{G} - B \right\|_F \leq \varepsilon; \tag{6}$$

where $\|\cdot\|_F$ is the Frobenius matrix norm, $\|\cdot\|_{2,1}$ is a mixed norm (sum of the L_2 norms of the rows of a matrix), and H is constructed by concatenating the signals (column vectors) side by side as follows

$$H = [\ H_{hh} \quad H_{vv} \quad H_{hv}\ ]; \tag{7}$$

where

$$H_{hh} = [\ g_{hh1} \quad g_{hh2} \quad \cdots \quad g_{hhP}\ ], \tag{8}$$

$$H_{vv} = [\ g_{vv1} \quad g_{vv2} \quad \cdots \quad g_{vvP}\ ], \tag{9}$$

$$H_{hv} = [\ g_{hv1} \quad g_{hv2} \quad \cdots \quad g_{hvP}\ ]. \tag{10}$$

Intuitively, the $L_{2,1}$ norm promotes sparsity along rows, while minimizing the energy along columns. As a result, the solution will be an ensemble of signals with significant overlap, which allows for polarimetric analyses. As a matter of fact, the authors in [6] proved that the probability of recovery failure decays exponentially in the number of columns of H. This improvement can be understood from the fact that a mixed norm regularization rules out many of the possible subspaces where our solution might lie, thereby reducing the degrees of freedom in the optimization.

In practice, we may want to rephase every element of B, so that all pixels have a flat earth phase component based on the distance to the center of the window of size Δx, Δr. Thus,

$$\Phi = \Phi_1 = \Phi_2 = \Phi_3 = \ldots = \Phi_p, \tag{11}$$

which not only makes computations easier but also provides more accurate results.

4. EXPERIMENTAL RESULTS

In order to demonstrate the potential of the DCS approach, we used TerraSAR-X data acquired over the city of Osaki, Japan. It consists of a stack of 33 dual-polarimetric corregisterd images taken in high-resolution spotlight mode. Specifically, the resulting range and azimuth resolution was 1 m and 2 m, respectively. As depicted in Fig. 1, the baseline distribution presents a total tomographic aperture of around 250 m. As regards the temporal baselines, the first image was acquired on April 20, 2009, whereas the last one on October 22, 2010. Due to this large gap between acquisitions, the phase calibration of the data required the determination of stable points in amplitude and phase. This selection was performed according to [8].

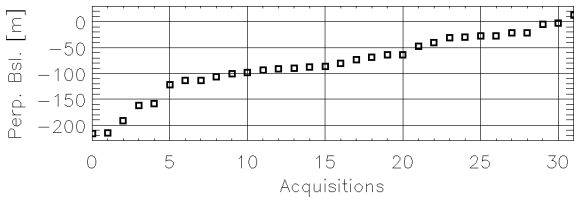

Figure 1. Perpendicular baseline distribution.

As shown in Fig. 2, the area of interest consists of an isolated building surrounded by agricultural fields. From Fig. 3, the height of the building can be estimated at 15 m - 20 m. Fig. 4 presents the corresponding SAR SLC dual-polarimetric image, together with a slice along azimuth that we analyzed for tomographic reconstruction. In particular, we used the methodologies previously described for 120 contiguous azimuth positions. As a result, we obtained tomograms in the azimuth and elevation directions of dimensions 240 m by 40 m, respectively.

In Fig. 5 (a) and (b), we took a 9 by 1 azimuth-range window and processed the tomograms individually for every

Figure 2. Optical image of the area of interest (©Google).

Figure 3. Image of the building reconstructed by means of SAR tomography (©Google). Its height can be estimated at 15 m - 20 m.

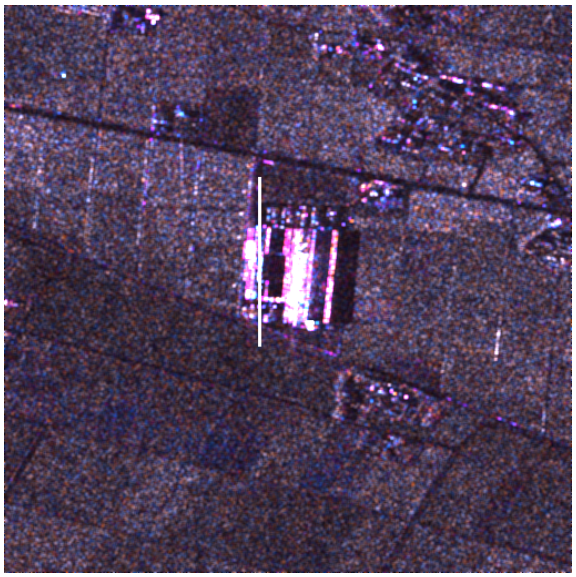

Figure 4. Master SLC dual-polarimetric image of the area of interest. Color code: R: VV, B: HH. The tomographic processing was carried out in the azimuth direction along the white line.

azimuth-range position and for each polarimetric channel. For instance, for the hh channel we solved

$$\min_{\widetilde{g}_{hhp}} \|\widetilde{g}_{hhp}\|_1 \text{ subject to } \|\Phi_p \widetilde{g}_{hhp} - b_{hhp}\|_2 \leq \varepsilon \quad (12)$$

for every p such that $1 \leq p \leq 9$. In Fig. 5 (a), the average intensities are displayed per polarimetric channel (R: VV, B: HH). In Fig. 5 (b), we added the resulting average intensities together at a specific elevation for all polarimetric channels. In Fig. 5 (c) and (d), we took again a 9 by 1 azimuth-range window but did the processing according to (6) for all azimuth-range positions and polarimetric channels. Evidently, Fig. 5 (c) and (d) exhibit a much clearer structure than Fig. 5 (a) and (b).

In order to emphasize the quality of the reconstruction, Fig. 6 presents the same results as Fig. 5 but no averaging is performed. In other words, only the reconstructed profile at the center of the azimuth-range window is displayed. Clearly, Fig. 6 (c) and (d) retain the main structural characteristics while Fig. 6 (a) and (b) degrade significantly.

5. CONCLUSIONS

A Distributed Compressed Sensing approach for polarimetric SAR tomography makes it possible to significantly improve the quality of the estimated sparse elevation profiles. In fact, it confers a distinct advantage, especially in the presence of large temporal baselines, as is the case for the spaceborne data analyzed in this work.

In effect, even though the elevation profiles for each azimuth-range pixel are separately encoded, joint recovery of ensembles of polarimetric reflectivity functions allows exploiting their shared information. In addition, the methods outlined allow for a robust polarimetric analysis of sparse solutions.

In the same spirit, a direct benefit of reducing the number of required passes is the possibility of studying the anisotropic behavior of scatterers in the elevation direction, since high resolution can be achieved using many small overlapping subapertures.

Future work will focus on including additional regularizations for targets that might not be sparse in the space domain, such as forests. As a matter of fact, elevation profiles are still extremely simple as compared with the behavior of the reflectivity function along azimuth and range. Hence, we are likely to find sparsifying bases, which may allow for analysis in the presence of volumetric scattering.

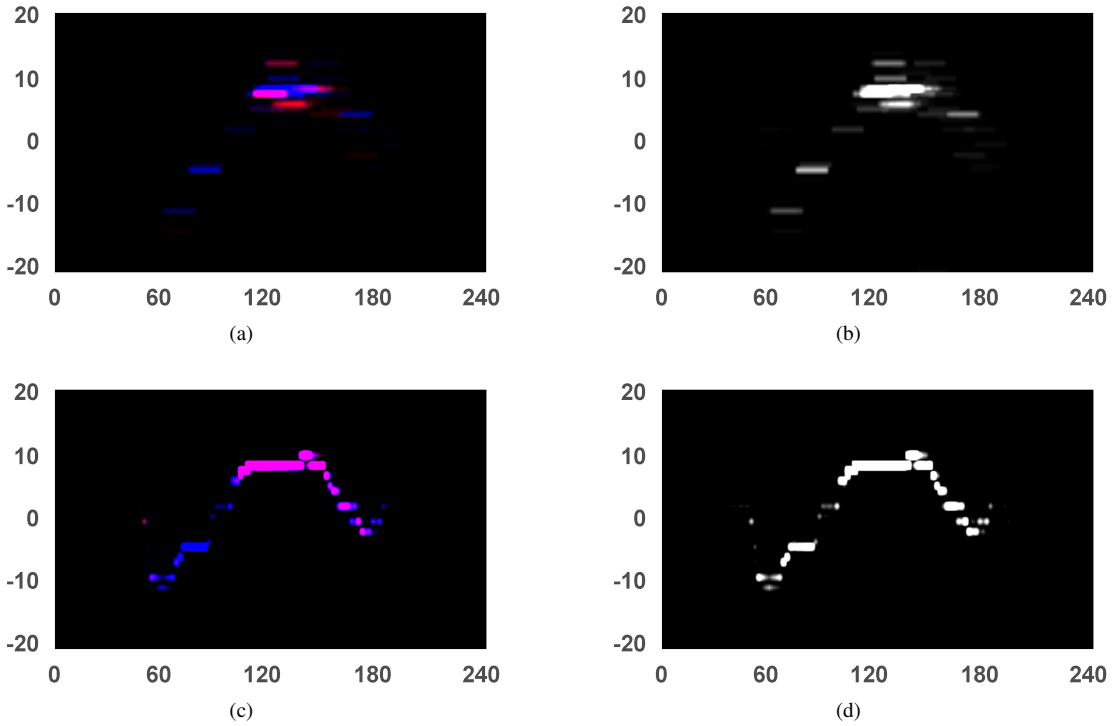

Figure 5. Comparison between CS and DCS (240 m by 40 m) using 33 passes and a 9 by 1 azimuth-range window: (a) Average intensities per polarimetric channel for CS; (b) Average span for CS; (c) Average intensities per polarimetric channel for DCS; (d) Average span for DCS.

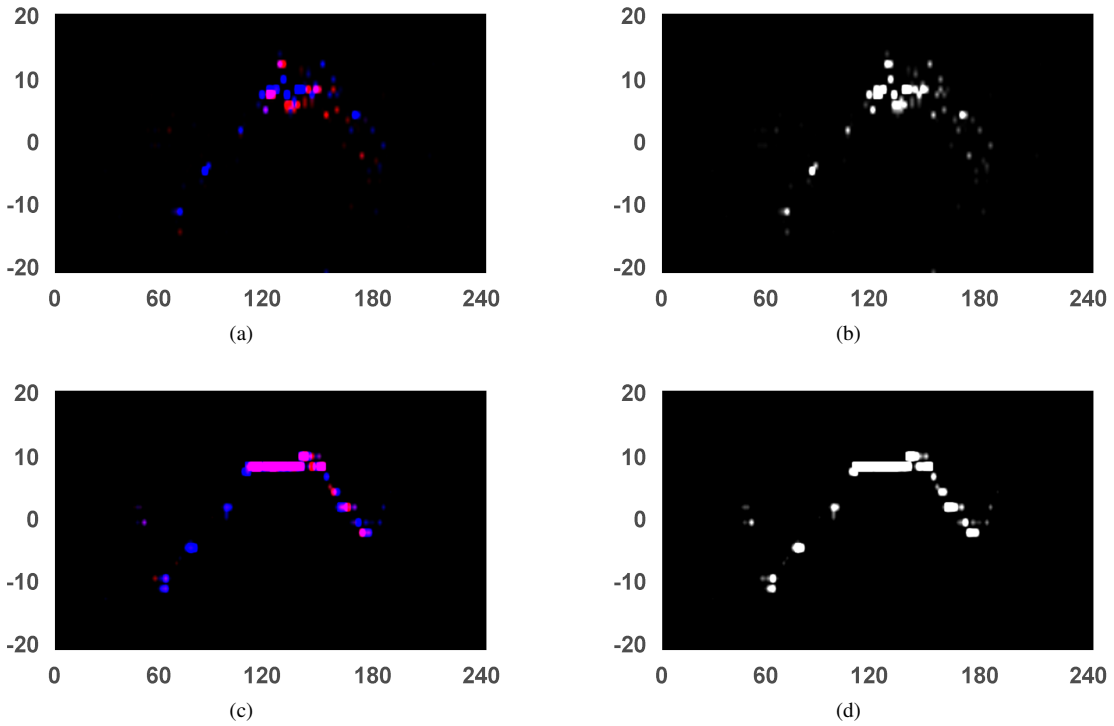

Figure 6. Comparison between CS and DCS (240 m by 40 m) using 33 passes and a 9 by 1 azimuth-range window. The plots show the reconstructed profiles at the center of the window (no averaging is carried out): (a) Intensities per polarimetric channel for CS; (b) Span for CS; (c) Intensities per polarimetric channel for DCS; (d) Span for DCS.

REFERENCES

[1] R. Baraniuk. Compressive sensing. *IEEE Signal Process. Mag.*, 24:118–121, Jul. 2007.

[2] D. Baron, M. Duarte, M. Waking, S. Sarvotham, and R. Baraniuk. Distributed compressive sensing. *Preprint*, 2009.

[3] E. Candès. Compressive sampling. *in Proc. Int. Congr. Math., Madrid, Spain*, 3:1433–1452, 2006.

[4] E. Candès, J. Romberg, and T. Tao. Robust uncertainty principles: exact signal reconstruction from highly incomplete frequency information. *IEEE Trans. Inf. Theory*, 52:489–509, Feb. 2006.

[5] D. Donoho. Compressed sensing. *IEEE Trans. Inf. Theory*, 52:1289–1306, Apr. 2006.

[6] Y.C. Eldar and H. Rauhut. Average case analysis of multichannel sparse recovery using convex relaxation. *IEEE Trans. Inf. Theory*, 56:505–519, Jan. 2010.

[7] S. Tebaldini. Algebraic synthesis of forest scenarios from multibaseline PolInSAR data. *IEEE Trans. Geosci. Remote Sens.*, 47:4132–4142, Dec. 2009.

[8] S. Tebaldini and A.M. Guarnieri. On the role of phase stability in SAR multibaseline applications. *IEEE Trans. Geosci. Remote Sens.*, 48(7):2953–2966, 2010.

[9] X.X. Zhu and R. Bamler. Tomographic SAR inversion by L1-norm regularization - The compressive sensing approach. *IEEE Trans. Geosci. Remote Sens.*, 48:3839–3846, Oct. 2010.